Heliyon

Received:
13 December 2018
Revised:
8 March 2019
Accepted:
1 April 2019

Cite as:
Muhammad Akhsin Muflikhun, Marcel C. Frommelt, Madiha Farman, Alvin Y. Chua, Gil Nonato C. Santos. Structures, mechanical properties and antibacterial activity of Ag/TiO_2 nanocomposite materials synthesized via HVPG technique for coating application.
Heliyon 5 (2019) e01475.
doi: 10.1016/j.heliyon.2019.e01475

Structures, mechanical properties and antibacterial activity of Ag/TiO_2 nanocomposite materials synthesized via HVPG technique for coating application

Muhammad Akhsin Muflikhun [a,*], Marcel C. Frommelt [b], Madiha Farman [c], Alvin Y. Chua [d], Gil Nonato C. Santos [e]

[a] *Department of Mechanical and Industrial Engineering, Faculty of Engineering, Gadjah Mada University, Jl. Grafika No. 2, Yogyakarta 55281, Indonesia*

[b] *University of Stuttgart, Stuttgart, Germany*

[c] *Mechanical Engineering Department, Khalifa University, Abu Dhabi, United Arab Emirates*

[d] *Mechanical Engineering Department, De La Salle University, 2401, Taft Avenue, Manila, Philippines*

[e] *Physics Department, De La Salle University, 2401, Taft Avenue, Manila, Philippines*

[*] Corresponding author.

E-mail address: akhsin.muflikhun@ugm.ac.id (M.A. Muflikhun).

Abstract

In this study, the structures and mechanical properties of the silver-titanium dioxide nanocomposite material were investigated using Atomic Force Microscopy (AFM). These properties include surface roughness, hardness, and reduced Young's modulus. The nanocomposite material was successfully synthesized using the Horizontal Vapor Phase Growth (HVPG) technique which yielded shapes such as nanoparticles, nanospheres, nanorods, triangular nanocomposites, and nanocrystals. Characterization of nanocomposite materials was done through Scanning Electron Microscopy (SEM) and Energy Dispersive X-ray (EDX)

https://doi.org/10.1016/j.heliyon.2019.e01475

spectroscopy to elucidate material shape, diameter, and composition. The pour plate technique combined with McFarland standards was used to evaluate the antibacterial activity of the nanocomposite material against *Staphylococcus aureus*. The nanocomposite material was able to eradicate bacteria and was suitable for coating applications effectively.

Keywords: Nanotechnology, Materials science, Mechanical engineering

1. Introduction

Recently, much research has been conducted into exploring the field of nanotechnology. Studies focus on the components, applications, characterization, and synthesis methods in order to obtain the best nanomaterials with optimal mechanical and physical properties, which are vastly different compared to macro-scale materials.

Many nanomaterials are used in medical applications or coating due to their excellent properties against bacteria. Silver-based nanomaterials are known for their antibacterial activity, as they generally possess excellent mechanical properties and can release heavy metal ions to cause damage to bacterial DNA. Various methods for the synthesis of silver nanomaterials have already been investigated and proven satisfactory; shapes obtained include nanoparticles, nanorods, triangular nanocomposites, and nanospheres [1, 2, 3, 4, 5]. On the other hand, silver and titanium dioxide nanomaterials have been explored by many researchers as they can be synthesized through various methods, including Sol-Gel, Micelle, and Inverse Micelle, Hydrothermal, Solvothermal, Electrodeposition, Chemical Vapor Deposition, Physical Vapor Deposition, HVPG, and Sonochemical [6, 7, 8, 9, 10, 11, 12].

Titanium dioxide containing different amounts of silver was synthesized by sol-gel methods in which the silver can be incorporated by irradiating the reaction mixture during preparation. The silver is homogeneously dispersed throughout the material and thus a more effective photocatalytic material can be produced. The efficiency of the materials can also be examined by a Q-Sun solar simulator. The results revealed that the addition of a higher amount of silver significantly increases the rate of degradation of a model dye (R6G). This phenomenon can be attributed to the increasingly visible absorption capacity of silver nanoparticles [13]. The other result is that the Ag/TiO_2 core-shell nanowires were successfully synthesized where the thickness of titanium dioxide coating is about 10 nm. This results showed good photocatalytic activities [14].

The Photoreduction method was used to modify TiO_2 with Ag nanoparticles. The TiO_2/Ag nanocomposites were used for water purification and disinfection of *E. coli* under ultraviolet (UV) irradiation. The study reported that metallic Ag nanoparticles were firmly immobilized on the TiO_2 surface and by improving the electron-

https://doi.org/10.1016/j.heliyon.2019.e01475

hole separation at the TiO_2/Ag interface. The nanocomposites were reported to be stable and could be repeatedly used under UV irradiation [15].

Besides photocatalytic and water purification, silver-titanium dioxide nanocomposite materials have been found to be effective for various applications, such as medical and dental technology [7, 16, 17, 18], virus inactivation [19], self-cleaning applications [20, 21], Photovoltaic cells [4], and food industry applications, including food processing, food packaging, nutraceutical delivery, and food safety/sensing [22].

There are different methods for synthesizing silver-titanium dioxide nanocomposites with high purity yields. However, the mechanical and physical properties of silver-titanium dioxide nanocomposites still need to be investigated further. This study strives to rectify the lack of data and research regarding the mechanical properties of silver-titanium dioxide nanocomposites. Data harvesting of mechanical properties utilizes SEM-AFM for surface roughness and AFM for hardness and reduced Young's modulus. The hardness of the silver-titanium dioxide nanocomposite is obtained from instrument indentation of the AFM tip and the contact area that strikes the material. The reduced Young's modulus is obtained from slope calculations during indentation load and displacement. Measurements are taken during loading and unloading [23, 24, 25].

As an antibacterial agent, silver-titanium dioxide nanocomposite materials are widely known for their anti-pathogenic ability; studies have reported efficacy against various strains of Gram-positive bacteria (*B. subtilis*, *S. aureus*, MRSA), Gram-negative bacteria (*E. coli*, *K. pneumonia*, *P. aeruginosa*), and fungi (*C. albicans*) [2, 26, 27, 28].

Additionally, it should be mentioned that previous studies regarding synthesis of nanomaterials often required the use of aggressive chemical materials as reducing agent, like hydrazine [29], sodium hydroxide, sodium borohydride, and hydrochloric acid [30]. Although these methods were reported to be successful in producing pure and well-defined nanoparticles, the cost-efficiency and environmental damage is not comparable and relatively high. Consequently, there is a need for development of more cost-effective and environmentally friendly methods. The choice of synthesis nanomaterials with free solvent system, free from reducing agent, and free from hazardous capping agent is one of the main reasons why we used the presented methods. This study aims to explore and reveal the mechanical properties of silver and titanium dioxide nanocomposite materials with anti-bacterial capabilities. In our current study, we present a simple horizontal vapor phase growth (HVPG) technique to synthesize Ag/TiO_2 nanocomposites. This technique was able to eliminate the pollutant and guarantee the purity of the nanocomposites because it is sealed in the vacuum tube, and as such can be considered an effective and environmentally friendly synthesis method for such nanocomposites - even more so since it only uses non-

https://doi.org/10.1016/j.heliyon.2019.e01475

aggressive chemical materials. In addition, it is a one-pot method with significantly fewer steps than solution-based techniques.

2. Materials and methods

A schematic of the materials preparation and laboratory experimentation in this study is shown in Fig. 1. An amount of 17.5 mg − each of silver powder and titanium dioxide − was measured out on a digital weighing scale, mixed and placed in quartz tubes sealed on one end.

The sealing process was carried out in the vacuum machine under low pressure in order to remove pollutants or contaminants and increase purity. After sealing, the tube was then baked in the furnace under specific parameters. Analysis of the nanocomposite materials was then done through SEM-EDX and AFM. The best parameters for baking were selected based on the diameter and shape of the materials. Lastly, the nanomaterial was tested using the pour plate technique to determine the efficacy of its anti-bacterial activity.

2.1. Synthesis of nanocomposites

The HVPG technique was used in this study to synthesize silver-titanium dioxide nanomaterials. The procedure for HVPG is shown in Fig. 2.

The Same amounts of Silver powder (99% purity) from Aldrich and titanium dioxide powder from Degussa P25 were measured (17.5mg each) (Fig. 2(a)). Both materials were then placed in a quartz tube sealed on one end and were then manually mixed (Fig. 2(b)). After mixing, the quartz tube was placed vertically in the High Vacuum machine and set to a pressure of 10^{-6} Torr $\approx 1.3 \times 10^{-4}$ Pa (Fig. 2(c)).

After being placed in the low-pressure machine and having both ends sealed, the quartz tube was then placed horizontally inside the furnace and the temperature was adjusted for the baking process (Fig. 2(d)). This study used a total of 27 combinations of different settings for the parameters of temperature, baking time, and zones, necessitating 9 different tubes. The tube configuration is shown in Fig. 2(e).

Table 1 summarizes the parameters for the study: there are three growth temperatures (800 °C, 1000 °C, and 1200 °C) and three baking times (4 hours, 6 hours, and 8 hours). Each quartz tube is further divided into 3 zones, which leads to 27 possible combinations in total.

2.2. Characterization of nanocomposite

SEM-EDX spectroscopy was used to characterize the silver-titanium dioxide nanocomposite materials. SEM was used to determine the shape and measure the diameter

https://doi.org/10.1016/j.heliyon.2019.e01475

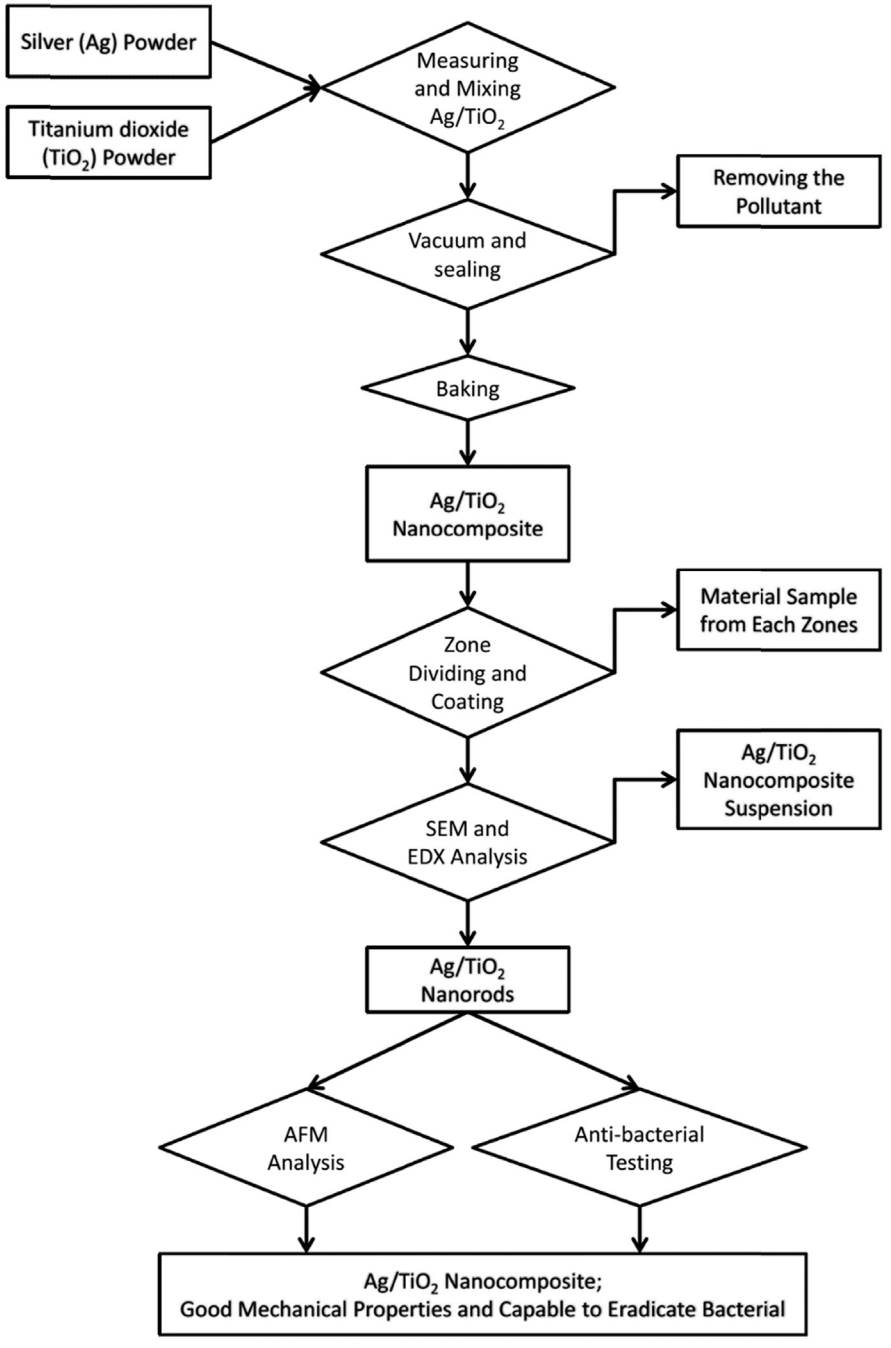

Fig. 1. Experimental flowchart.

of the nanocomposites. The measurement technique used three samples with different spots in a single zone. EDX spectroscopy was used to conduct an elemental analysis, especially to quantify the amount of silver and titanium dioxide in each setup, therefore giving the percentage of each component. From SEM, the optimal combination of parameters can be determined, and the one selected to produce the best results underwent AFM to determine mechanical properties. SEM in this study

https://doi.org/10.1016/j.heliyon.2019.e01475

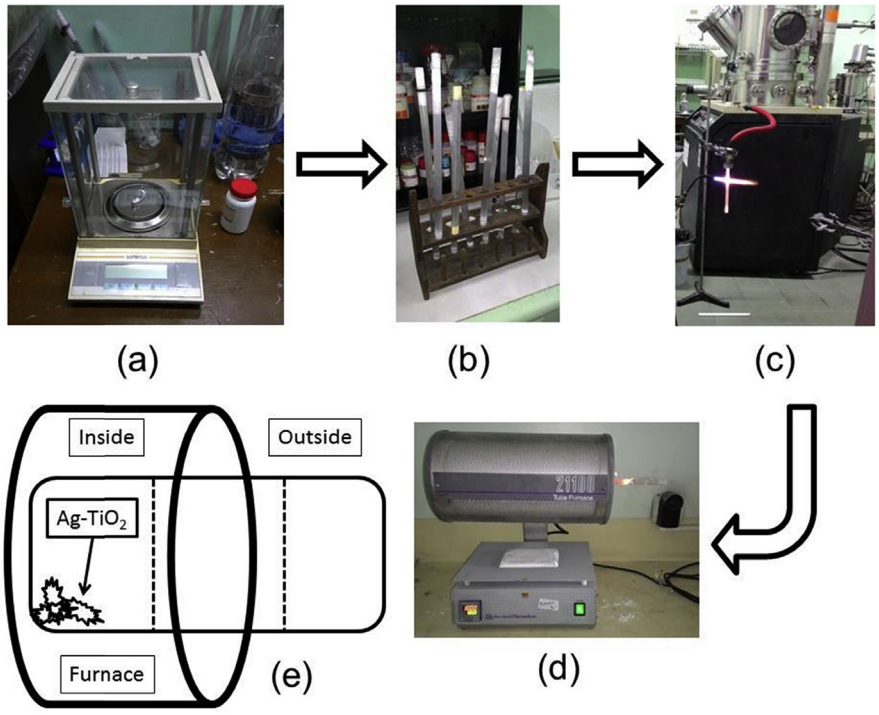

Fig. 2. HVPG schematic: (a) Measuring material, (b) Mix and sealing material, (c) Vacuuming and permanent sealing of both ends of the quartz tube, (d) Baking materials in the horizontal furnace, (e) Tube placement and position.

was used JEOL 5310 type and EDX (Oxford with Link Isis). The AFM used XE100 from Park system and the test was obtained at the Sigmatech Inc. The Philippines.

2.3. Anti-bacterial test

An anti-bacterial test was used in this study to investigate the silver-titanium dioxide nanocomposite material's efficacy in eradicating bacteria. The method used was the

Table 1. Study parameters.

Sample	Temp. (°C)	Time (h)	zone	Sample	Temp. (°C)	Time (h)	zone	Sample	Temp. (°C)	Time (h)	zone
1	800	4	1	10	1000	4	1	19	1200	4	1
2			2	11			2	20			2
3			3	12			3	21			3
4		6	1	13		6	1	22		6	1
5			2	14			2	23			2
6			3	15			3	24			3
7		8	1	16		8	1	25		8	1
8			2	17			2	26			2
9			3	18			3	27			3

https://doi.org/10.1016/j.heliyon.2019.e01475

pour plate technique with dilution factors from 10^{-1} until 10^{-6} and subsequently counting bacterial colonies based on the 0.5 McFarland standard.

Fig. 3 shows a schematic for the anti-bacterial testing. The 0.5 McFarland standard was used to compare turbidity between 0.5 McFarland standards with the bacterial culture. The 0.5 McFarland was prepared with 1% barium chloride and 1% sulfuric acid in a ratio of 0.05:9.95. The approximate total amount of cell density based on the 0.5 McFarland standard was 1.5×10^8 CFU/mL (Fig. 3(a)).

Around 5 ml of the bacterial culture was then poured into three different tubes, with two tubes containing the silver-titanium dioxide nanocomposite and one tube empty, as shown in Fig. 3(b). From each tube, 1 ml was then transferred to another tube with 9 ml of sterilized water (Fig. 3(c)), constituting the 10^{-1} dilution. Serial dilutions were then carried out until a dilution factor of 10^{-6} was obtained.

From each dilution tube, 1 μl (1 microliter) of liquid was then transferred to three petri-dishes as shown in Fig. 3(d), resulting in 18 dishes per tube, for a total of 54. The set-ups were then isolated for 18 hours before performing analysis through counting the number of bacterial colonies in each petri dish (Fig. 3(e)).

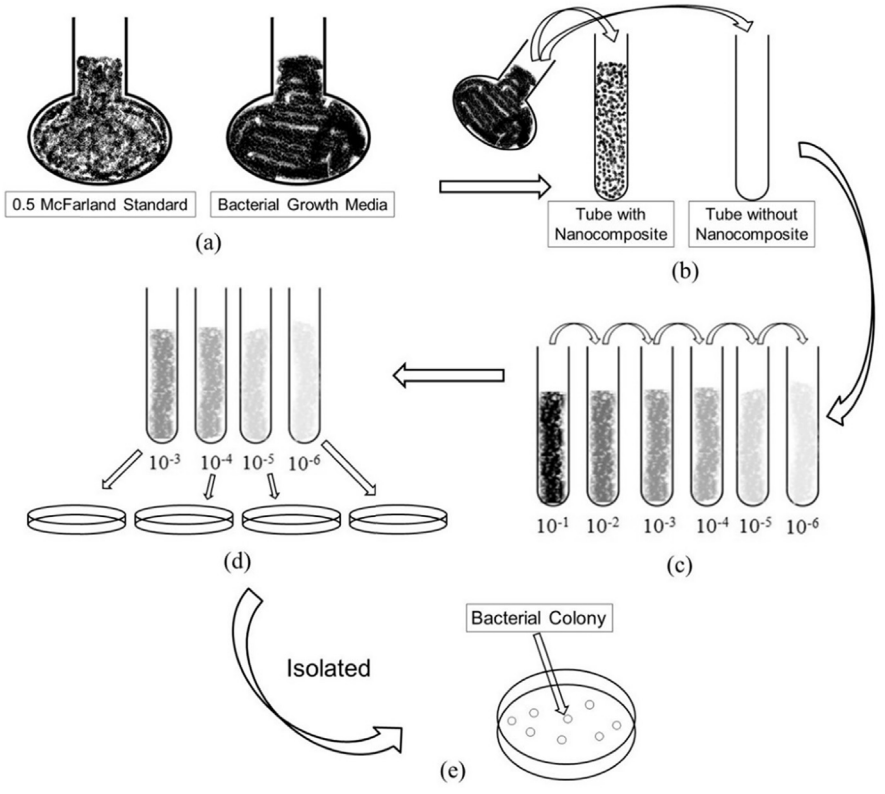

Fig. 3. Antibacterial performance test schematic: (a) comparing bacterial colonies with 0.5 McFarland standard, (b) bacterial colonies poured into quartz tube with and without Nanocomposites, (c) tubes diluted with dilution factors from 10^{-1} to 10^{-6}, (d) transfer of culture to petri dish, (e) After isolation, the bacterial colonies appeared in the petri dish counted manually.

https://doi.org/10.1016/j.heliyon.2019.e01475

3. Theory

3.1. HVPG technique

The material undergoes several changes as it passes the various stages of HVPG. The materials start in solid form on the macro scale. As they bake horizontally in the furnace, the materials slowly change from solid to liquid (at the melting point) and then to gas (at the boiling point). These changes are reversed as the materials slowly cool down to lower temperatures during condensing and time-adhering to the surface of the quartz tube as a liquid with various sizes, shapes and diameters and in the final process, the materials were completely stable at the nano-solid scale. The materials conversion schematic is shown in Fig. 4.

3.2. Hardness

AFM was used in this study to investigate the hardness of the silver-titanium dioxide nanocomposite material. The hardness of the Ag/TiO_2 was computed based on the Eq. (1) [31, 32].

$$H = \frac{P_{max}}{A} \tag{1}$$

where H is the hardness of the silver-titanium dioxide nanocomposite (kPa), P_{max} is the maximum load (N), and A is the projected area used on the indenter during AFM test (m^2).

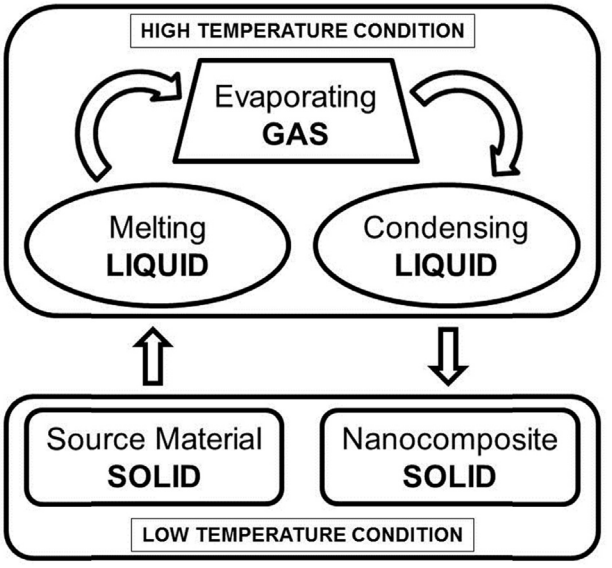

Fig. 4. Material conversion in HVPG.

https://doi.org/10.1016/j.heliyon.2019.e01475

3.3. Reduced Young's modulus

The reduced Young's modulus can be calculated from the Eqs. (2) and (3) [31, 32].

$$E_r = \frac{\sqrt{\pi}}{2} \times \frac{s}{\sqrt{A}} \tag{2}$$

$$s = \left.\frac{dp}{dh}\right|_{P_{\max}} \tag{3}$$

where s is the slope from the indentation $\left(\frac{nN}{nm}\right)$ and E_r is the reduced Young's modulus (kPa), and A is the projected area used on the indenter during AFM test (m^2).

4. Results and discussion

4.1. SEM and EDX

Fig. 5 shows The SEM images of Ag dan TiO_2 macro material (source material). The representative sample of all 9 tubes specimens are presented in Fig. 6. The images clearly show that the Ag/TiO_2 was deposited at the tube surface. However, in the 4 hours of baking time and 800 °C of growth temperature, the Ag/TiO_2 materials have not fully changed to the nano-scale. It may be due to insufficient temperature and baking time to evaporate Ag/TiO_2. The smallest size of Ag/TiO_2 is obtained from the 8 hours of baking time and 1000 °C growth temperature with the nanorod shape being an advantage as it physically eradicates bacterial by breaking its

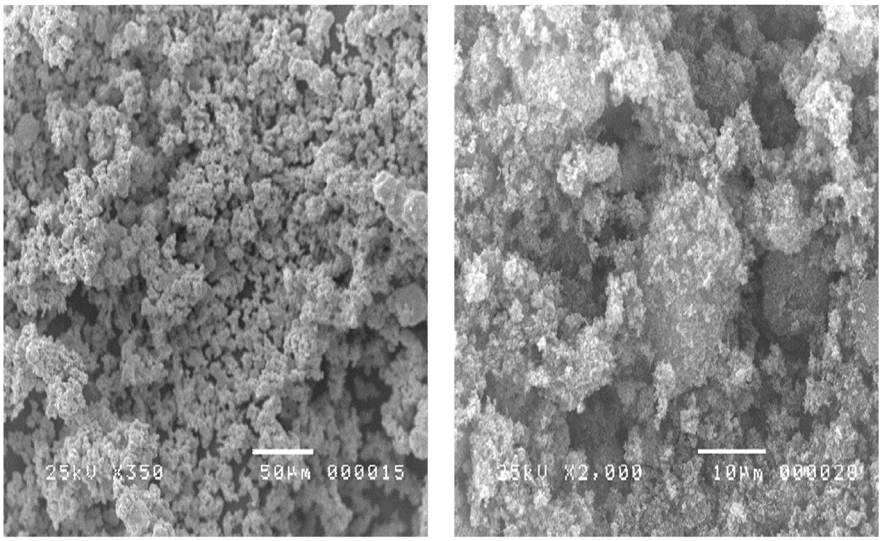

Fig. 5. SEM images of (a) Ag macro material, and (b) TiO_2 macro material.

https://doi.org/10.1016/j.heliyon.2019.e01475

membranes. For all parameter combinations, SEM imaging was used to determine the shape and diameter of nanocomposites.

Fig. 7 shows the distribution of diameter measurements of the silver-titanium dioxide nanocomposite material for all 27 parameter configurations. The measured diameters varied in scale from micro size (24.8 μm) to nano-scale (0.22 nm). From Fig. 7 the diameters of the synthesized nanocomposites are widely distributed, ranging from micrometer to nanometer level. The wide range is caused by material that has not been fully synthesized, and the deposited material is unchanged (on the micro level). The micro-materials are also caused by titanium dioxide that is not fully converted into nano-scale materials.

In the previous studies, the type of materials and particle size used for coating as well as excellence in anti-bacterial performance are two important factors affecting the resulting antimicrobial efficiency and effectiveness. As an example, nanomaterials have different properties compared to the same materials with larger particles. In fact, surface or volume ratio of nanomaterials increases considerably with a decrease in the size. Furthermore, in the case of Ag/TiO_2 nanocomposites, it could interact with the bacterial membrane, leading to bacterial membrane damage, subsequently killing the bacteria. There are two methods of how Ag/TiO_2 eradicates bacteria. First, it would initially accumulate on the surface of the bacterial membrane, penetrate the bacteria, changing the permeability of the bacterial membrane and damage the membrane. Secondly, it assumes geometrical forms with sharp edges, such as triangular or rod shapes and breaks the bacterial membrane. These parameters of nanocomposites include size, shape, and surface. Particularly, it was found that nanomaterials with small sizes result in high efficacy in damaging the bacterial membrane, compared with the bigger size [2, 8, 18, 33, 34].

Based on the study, the determination of the best parameter was obtained by sorting the best combinations from SEM images and diameter measurement of nanocomposites from Fig. 6 and Fig. 7. The best combination was obtained for the tube with growth temperature 1000 °C and a baking time of 8 hours. Fig. 8 presents the SEM image and EDX analysis. It shows that the majority of the silver-titanium dioxide nanocomposites were shaped as nanorods. The EDX shows the presence of Si which are the quartz-tube materials as well as Au that represent gold as coating material before being placed inside the SEM machine.

The materials' shapes vary by zone in the different tubes. This data is summarized in Table 2. Geometrically, nanorods are the most promising shape for nanocomposite materials in terms of anti-bacterial capability as seen in Table 2, the quartz tube with a growth temperature of 1000 °C and a baking time of 8 hours had nanorods in all three zones. The setups numbered 16, 17 and 18 were the ones selected for further analysis via AFM and anti-bacterial activity because they contained nanorods in all zones, with zone 2 (No. 17) having the smallest range of nanocomposite diameters.

https://doi.org/10.1016/j.heliyon.2019.e01475

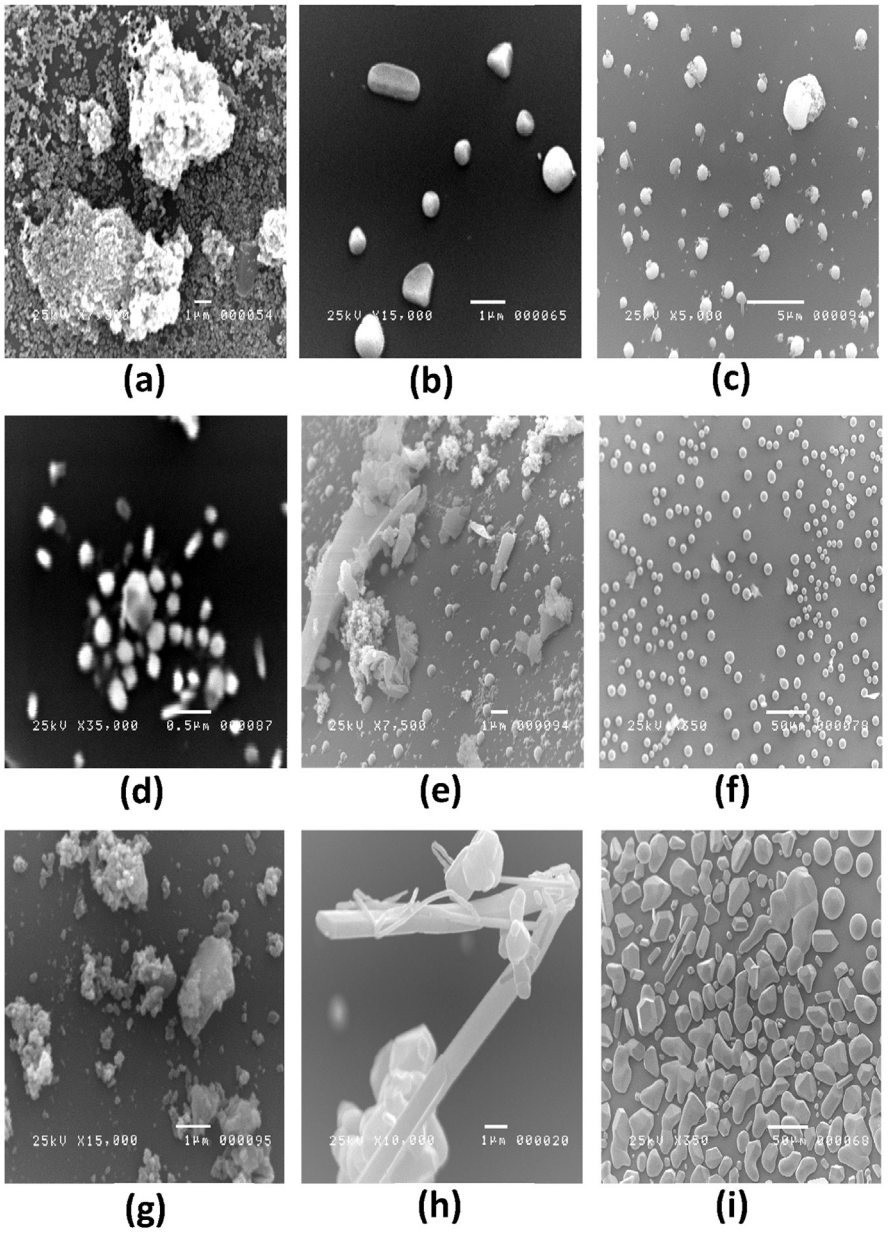

Fig. 6. Representative SEM images of Ag/TiO_2 nanocomposites. 4 hours baking time with (a) 800 °C growth temperature, (b) 1000 °C growth temperature, and (c) 1200 °C growth temperature. 6 hours baking time with (d) 800 °C growth temperature, (e) 1000 °C growth temperature, and (f) 1200 °C growth temperature. 8 hours baking time with (g) 800 °C growth temperature, (h) 1000 °C growth temperature, and (i) 1200 °C growth temperature.

4.2. AFM analysis

4.2.1. Surface roughness (3D)

AFM analysis was carried out on samples from the quartz tube with set-up no. 17, the parameters being a growth temperature of 1000 °C and 8 hours of baking

https://doi.org/10.1016/j.heliyon.2019.e01475

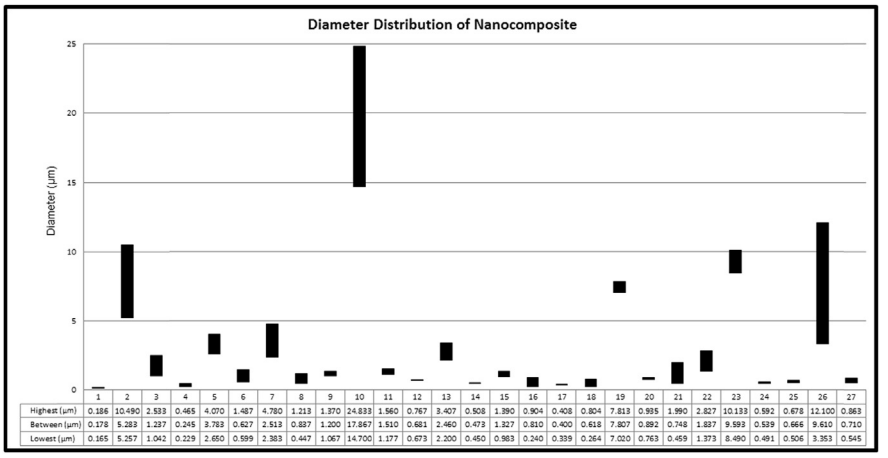

	1	2	3	4	5	6	7	8	9	10	11	12	13	14	15	16	17	18	19	20	21	22	23	24	25	26	27
Highest (µm)	0.186	10.490	2.533	0.465	4.070	1.487	4.780	1.213	1.370	24.833	1.560	0.767	3.407	0.508	1.390	0.904	0.408	0.804	7.813	0.935	1.990	2.827	10.133	0.592	0.678	12.100	0.863
Between (µm)	0.178	5.283	1.237	0.245	3.783	0.627	2.513	0.837	1.200	17.867	1.510	0.681	2.460	0.473	1.327	0.810	0.400	0.618	7.807	0.892	0.748	1.837	9.593	0.539	0.666	9.610	0.710
Lowest (µm)	0.165	5.257	1.042	0.229	2.650	0.599	2.383	0.447	1.067	14.700	1.177	0.673	2.200	0.450	0.983	0.240	0.339	0.264	7.020	0.763	0.459	1.373	8.490	0.491	0.506	3.353	0.545

Fig. 7. Diameter distribution of Ag/TiO_2 Nanocomposite across all parameters.

time. Fig. 9 shows the AFM result from quartz tube No. 17. The length of the material varied from 10.961 nm to 216 nm and the elevation of the nanorods ranged from 2.266 nm to 11.997 nm. The summary of the data gathered from AFM is shown in Fig. 10 for the diameter of the nanocomposites and Fig. 11 for their elevation.

Fig. 9 shows 2D and 3D images of surface roughness obtained from AFM. The results showed that AFM could be used as an efficient technique to determine the topography of Ag/TiO_2 nanocomposites. It is shown that the nanorod's structure was formed with a wider base than the top of the nanocomposites. This shows that TiO_2 grows in nano-scale cotton-like, and the Ag grows as silver-nanorods

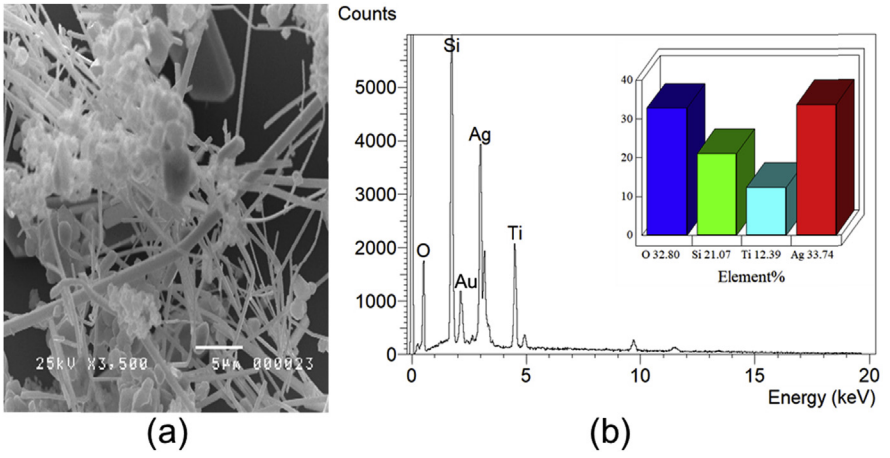

Fig. 8. (a) SEM image of Ag/TiO_2 nanocomposite from 8 hours baking time at 1000 °C, and (b) EDX of Ag/TiO_2 nanocomposite from 8 hours baking time at 1000 °C with the inset is the element percentages (O, Si, Ti, and Ag).

https://doi.org/10.1016/j.heliyon.2019.e01475

Table 2. Nanocomposite shapes in all study parameters.

No.	Temperature	Baking Time	Zone	Material Shape and diameter
1	800 °C	4 Hours	1	Nanoparticles
2			2	Microparticles
3			3	Microparticles
4		6 Hours	1	Nanospheres, Nanoparticles
5			2	Nanoparticles
6			3	Nanoparticles
7		8 Hours	1	Nanoparticles
8			2	Nanotubes, Nanospheres
9			3	Nanoparticles
10	1000 °C	4 Hours	1	Nanoparticles
11			2	Nanospheres, Nano-triangular, Nanorods
12			3	Nanospheres, Nano-triangular
13		6 Hours	1	Nanoparticles
14			2	Nanoparticles, Nanospheres
15			3	Nanoparticles
16		8 Hours	1	Nanoparticles, Nanorods
17			2	Nanorods, Nanoparticles
18			3	Nanorods, Nanoparticles
19	1200 °C	4 Hours	1	Nanoparticles
20			2	Nanospheres, Nanoparticles
21			3	Nanoparticles
22		6 Hours	1	Nanoparticles
23			2	Nanocrystal, Nano-triangular
24			3	Nanoparticles
25		8 Hours	1	Nanoparticles
26			2	Nanospheres, Nanorods, Nanocrystal
27			3	Nanorods

that are shown in Fig. 8. The nanocomposite materials are vertically positioned, allowing them to be able to disrupt bacterial cell membranes.

4.2.2. Hardness of nanocomposite

AFM was used to determine the hardness of the silver-titanium dioxide nanocomposite material. Hardness of Ag/TiO_2 nanocomposite was calculated using Eq. (1), and the result is shown in Eq. (4).

https://doi.org/10.1016/j.heliyon.2019.e01475

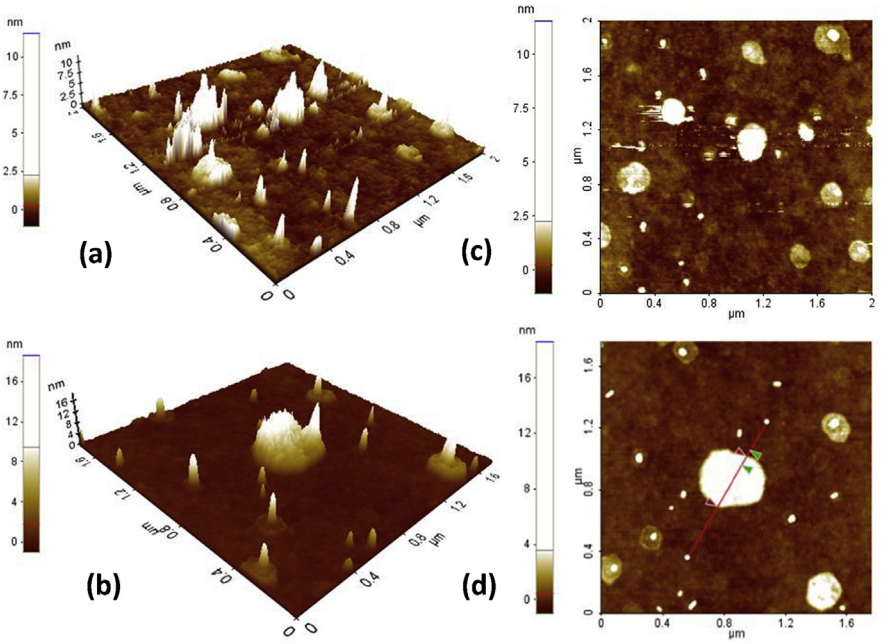

Fig. 9. (a) and (b) 3D image from AFM, (c) and (d) 2D image from AFM.

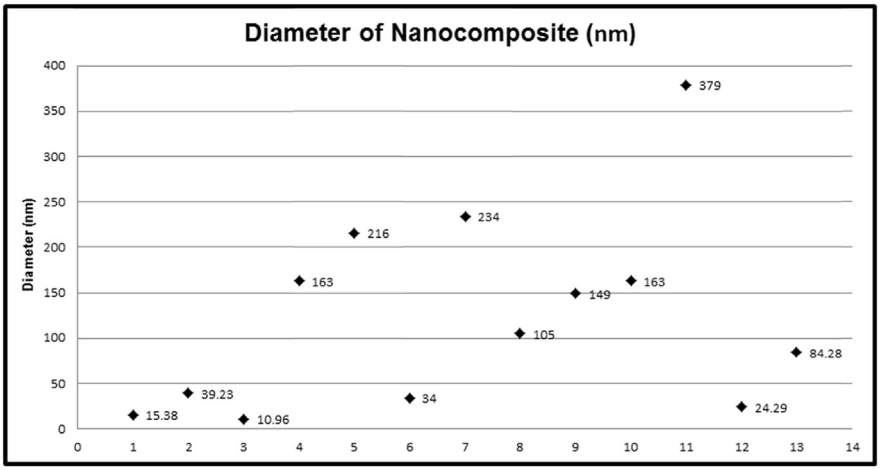

Fig. 10. Diameter measurement of Ag/TiO_2 Nanocomposite using AFM.

$$H = \frac{3.376 \times 10^{-9} N}{32 \times 10^{-12} m^2} = 105.5 Pa \tag{4}$$

where H is the hardness of the silver-titanium dioxide nanocomposite (kPa).

4.2.3. Reduced Young's modulus of nanocomposite

The reduced Young's modulus of the nanocomposite was determined through AFM and calculated using Eq. (2), and the result are shown in Eqs. (5) and (6).

https://doi.org/10.1016/j.heliyon.2019.e01475

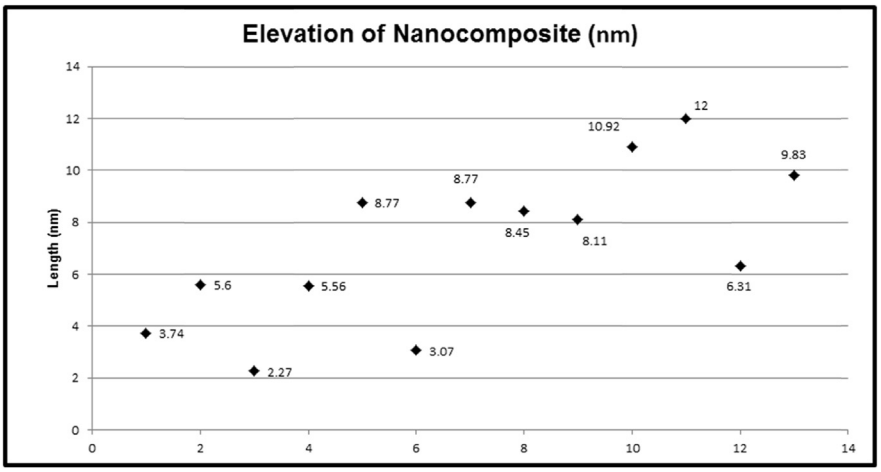

Fig. 11. Elevation measurement of Ag/TiO_2 Nanocomposite using AFM.

$$E_r = \frac{\sqrt{\frac{22}{7}}}{2} \times \frac{\frac{1.6nN}{42.95nm}}{\sqrt{32 \times 10^{-12}}} \tag{5}$$

$$E_r = 5.8kPa \tag{6}$$

where E_r is the reduced Young's modulus (kPa).

AFM analysis is used to analyze the surface topography of the samples containing Ag/TiO_2. By using AFM, the images obtained allow for calculation of the surface roughness and hardness of the material. The AFM analysis is a new analysis that used the HVPG technique to obtain the 3D image of nanocomposite. In this study it is shown that the combination between Ag/TiO_2 create sharp-end nanocomposites with the hardness of the composite being 105.5 Pa. The 3D shape of the nanocomposites is critical since in this study, the mechanism of nanocomposites eradicating bacteria relies on its form to break the bacterial membrane. The sharp ends of nanocomposites as confirmed by the bacterial test with Ag/TiO_2 are capable to eradicate bacteria by using its form. Similar studies are also reported from previous research [35, 36], which indicate that the sharp-end nano-structures are one of the main reasons for the effectiveness of nanocomposites against bacteria.

4.3. Pour plate technique

The pour plate technique was used to test the antibacterial activity of silver-titanium dioxide nanocomposite against *Staphylococcus aureus* with dilution factors of 10^{-1} to 10^{-6}. Fig. 12 shows the colony counts for the various set-ups with dilution factor 10^{-5}. A tube with nanocomposites can eradicate bacteria with promising results of more than 50 %. Moreover, by increasing the dilution factor to 10^{-6}, the results show

https://doi.org/10.1016/j.heliyon.2019.e01475

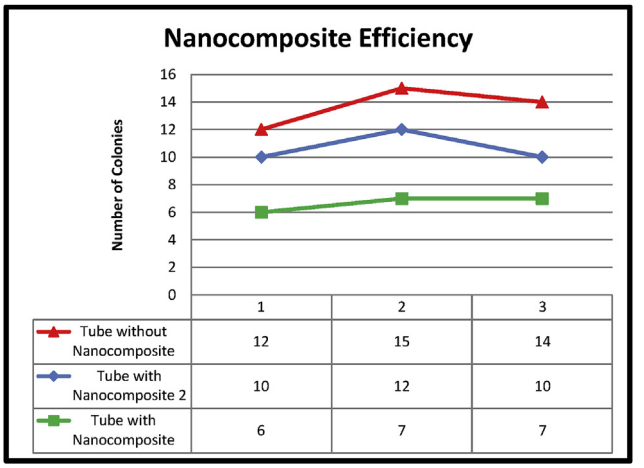

Fig. 12. Anti-bacterial test result.

that by using Ag/TiO_2 nanocomposites material, 100 % of the bacteria can be eradicated as shown in Fig. 13.

Comparing the present study with other studies, it can be noted that only few studies have been reported on the antibacterial eradication by nanomaterials in the shape of nanorods. Jan et al. [37] have reported synthesizing Ni doped ZnO nanorods by using analytical grade zinc chloride (ZnCl2), nickel chloride, acetic acid and NaOH that are capable to eradicate bacteria. Au nanorods synthesized using confined convective assembly methods have been observed by Zhu et al. [38]. The results show the nanorods can eradicate the bacterial in combination with laser irradiation. The Ag/TiO_2 nanorods were reported by He et al. [39] by using the Oblique Angle Deposition method. This method is similar to the HVPG technique since it used quartz tube sealed in a vacuum chamber annealed under high temperature. The results show the nanorods sizes are quite big, approximately 9 nanorods/μm^2 and without any antibacterial test result. Although the previous results show the nanorods were capable to eradicate bacteria, there is still lack of information about the

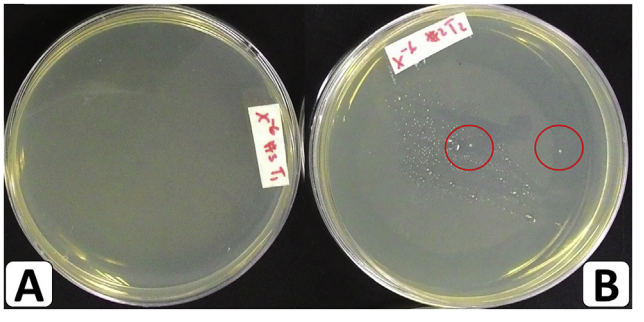

Fig. 13. Dilution factor 10^{-6} (A) with nanocomposites, and (B) without nanocomposites. The red circles indicate the bacterial colonies.

https://doi.org/10.1016/j.heliyon.2019.e01475

geometrical shape related to antibacterial properties. The present study shows the first analysis that establishes a relation between the nanorods' geometrical shape and bacteria in 3D shape by using AFM as well as calculating the hardness of the nanocomposite material. The present study shows that bacteria can be eradicated not only by releasing ion from the nanomaterials, but also by capability of eradicating bacteria using its shape.

5. Conclusions

The present study reports the successful synthesizing and characterization of the Ag/TiO_2 nanocomposites by using the HVPG technique. The study obtained the nanocomposites' structures, mechanical properties, and bacterial performance, which are important parameters for use in future applications such as medical, coating technology and filter applications. The study also revealed Ag/TiO_2 with various shapes such as nanoparticles, nanospheres, nanorods, nanotubes, triangular nanocomposites, and nanocrystals are successfully synthesized. Moreover, this study successfully produced nano-scale composite materials with unique shape (nanorods with sharp-ends) and can eradicate bacteria because of their geometrical shape. The length of the nanocomposites is varied from 10.9 nm to 216 nm and the elevation of the nanorods ranged from 2.3 nm to 12 nm with the hardness being 105.5 Pa. The results show sharp-end nanorods have an optimal geometry that can naturally break through the bacterial cell membrane, causing the bacterial cell to dry out and die. More importantly, the results from pour-plate technique demonstrate that Ag/TiO_2 with sharp-end nanorods are capable to eradicate bacteria with more than 50 % efficiency.

Declarations

Author contribution statement

Muhammad A. Muflikhun: Conceived and designed the experiments; Performed the experiments; Analyzed and interpreted the data; Contributed reagents, materials, analysis tools or data; Wrote the paper.

Marcel C. Frommelt, Madiha Farman: Analyzed and interpreted the data; Wrote the paper.

Alvin Y. Chua, Gil N.C. Santos: Conceived and designed the experiments; Contributed reagents, materials, analysis tools or data; Wrote the paper.

https://doi.org/10.1016/j.heliyon.2019.e01475

Funding statement

This work was supported by the Solid-State Physics Lab and 17 Microbiology Lab of De La Salle University and the AUN SEED-Net Grant.

Competing interest statement

The authors declare no conflict of interest.

Additional information

No additional information is available for this paper.

Acknowledgements

The authors thank Prof. Esperanza Cabrera and Gwen Castillon for their technical, experimental, and scientific support.

References

[1] P. Zhang, I. Wyman, J. Hu, S. Lin, Z. Zhong, Y. Tu, et al., Silver nanowires: synthesis technologies, growth mechanism and multifunctional applications, Mater. Sci. Eng. B Solid State Mater. Adv. Technol. 223 (2017) 1−23.

[2] M.J. Hajipour, K.M. Fromm, A. Akbar Ashkarran, D. Jimenez de Aberasturi, I.R. de Larramendi, T. Rojo, et al., Antibacterial properties of nanoparticles, Trends Biotechnol. 30 (2012) 499−511.

[3] M.A. Muflikhun, G.B. Castillon, G.N.C. Santos, A.Y. Chua, Micro and nano silver-graphene composite manufacturing via horizontal vapor phase growth (HVPG) technique, Mater. Sci. Forum 901 (2017) 3−7. Trans Tech Publications.

[4] O. Amiri, S. Bagheri, M. Mazaheri, M. Salavati-Niasari, M. Farangi, Stable plasmonic-improved dye sensitized solar cells by silver nanoparticles between titanium dioxide layers, Electrochim. Acta 152 (2014) 101−107.

[5] M. Goudarzi, N. Mir, M. Mousavi-Kamazani, S. Bagheri, M. Salavati-Niasari, Biosynthesis and characterization of silver nanoparticles prepared from two novel natural precursors by facile thermal decomposition methods, Sci. Rep. 6 (2016) 1−13.

[6] X. Chen, S.S. Mao, Titanium dioxide nanomaterials: synthesis, properties, modifications and applications, Chem. Rev. 107 (2007) 2891−2959.

[7] A. Besinis, T. De Peralta, R.D. Handy, The antibacterial effects of silver, titanium dioxide and silica dioxide nanoparticles compared to the dental

https://doi.org/10.1016/j.heliyon.2019.e01475

disinfectant chlorhexidine on Streptococcus mutans using a suite of bioassays, Nanotoxicology 8 (2014) 1−16.

[8] K. Zheng, M.I. Setyawati, D.T. Leong, J. Xie, Antimicrobial silver nanomaterials, Coord. Chem. Rev. 357 (2018) 1−17.

[9] M.A. Muflikhun, A.Y. Chua, G.N.C. Santos, Statistical design analysis of silver-titanium dioxide nanocomposite materials synthesized via horizontal vapor phase growth (HVPG), Key Eng. Mater. 735 (2017) 210−214.

[10] M.A. Muflikhun, G.N. Santos, A.Y. Chua, Synthesis and characterization of silver-titanium nanocomposite via horizontal vapor phase growth (HVPG) technique, DLSU Res. Congr. (2015) 1−5.

[11] F. Soofivand, F. Mohandes, M. Salavati-Niasari, Silver chromate and silver dichromate nanostructures: Sonochemical synthesis, characterization, and photocatalytic properties, Mater. Res. Bull. 48 (2013) 2084−2094.

[12] F. Mohandes, M. Salavati-Niasari, Sonochemical synthesis of silver vanadium oxide micro/nanorods: solvent and surfactant effects, Ultrason. Sonochem. 20 (2013) 354−365.

[13] M.K. Seery, R. George, P. Floris, S.C. Pillai, Silver doped titanium dioxide nanomaterials for enhanced visible light, photocatalysis 189 (2007) 258−263.

[14] S.F. Chin, S.C. Pang, F. Emmanuel, I. Dom, Sol-gel synthesis of silver/titanium dioxide (Ag/TiO_2) core-shell nanowires for photocatalytic applications, Mater. Lett. 65 (2011) 2673−2675.

[15] Z. Xiong, J. Ma, W.J. Ng, T.D. Waite, X.S. Zhao, Silver-modified mesoporous TiO2 photocatalyst for water purification, Water Res. 45 (2011) 2095−2103.

[16] A. Azam, A.S. Ahmed, M. Oves, M.S. Khan, S.S. Habib, A. Memic, Antimicrobial activity of metal oxide nanoparticles against Gram-positive and Gram-negative bacteria: a comparative study, Ijnm (2012) 6003−6009.

[17] A. Besinis, S.D. Hadi, H.R. Le, C. Tredwin, R.D. Handy, Antibacterial activity and biofilm inhibition by surface modified titanium alloy medical implants following application of silver, titanium dioxide and hydroxyapatite nanocoatings, Nanotoxicology 11 (2017) 327−338.

[18] M. Samiei, A. Farjami, S.M. Dizaj, F. Lotfipour, Nanoparticles for antimicrobial purposes in Endodontics: a systematic review of in vitro studies, Mater. Sci. Eng. C 58 (2016) 1269−1278.

https://doi.org/10.1016/j.heliyon.2019.e01475

[19] M.V. Liga, E.L. Bryant, V.L. Colvin, Q. Li, Virus inactivation by silver doped titanium dioxide nanoparticles for drinking water treatment, Water Res. 45 (2011) 535−544.

[20] C. Srisitthiratkul, V. Pongsorrarith, N. Intasanta, The potential use of nanosilver-decorated titanium dioxide nanofibers for toxin decomposition with antimicrobial and self-cleaning properties, Appl. Surf. Sci. 257 (2011) 8850−8856.

[21] K. Laohhasurayotin, S. Pookboonmee, Multifunctional properties of Ag/TiO 2/bamboo charcoal composites : preparation and examination through several characterization methods, Appl. Surf. Sci. 282 (2013) 236−244.

[22] C.F. Chau, S.H. Wu, G.C. Yen, The development of regulations for food nanotechnology, Trends Food Sci. Technol. 18 (2007) 269−280.

[23] W.C. Oliver, G.M. Pharr, Measurement of hardness and elastic modulus by instrumented indentation: advances in understanding and refinements to methodology, J. Mater. Res. 19 (2004) 3−20.

[24] M. Sebastiani, K.E. Johanns, E.G. Herbert, G.M. Pharr, Measurement of fracture toughness by nanoindentation methods: recent advances and future challenges, Curr. Opin. Solid State Mater. Sci. 19 (2015) 324−333.

[25] C. Feng, B.S. Kang, Young's modulus measurement using a simplified transparent indenter measurement technique, Exp. Mech. 48 (2008) 9−15.

[26] M. Lungu, Silver − titanium dioxide nanocomposites as effective antimicrobial and antibiofilm agents, J. Nanopart. Res. 16 (2014) 1−15.

[27] S. Mei, H. Wang, W. Wang, L. Tong, H. Pan, C. Ruan, et al., Antibacterial effects and biocompatibility of titanium surfaces with graded silver incorporation in titania nanotubes, Biomaterials 35 (2014) 4255−4265.

[28] F.C. Yang, K.H. Wu, J.W. Huang, D.N. Horng, C.F. Liang, M.K. Hu, Preparation and characterization of functional fabrics from bamboo charcoal/silver and titanium dioxide/silver composite powders and evaluation of their antibacterial efficacy, Mater. Sci. Eng. C 32 (2012) 1062−1067.

[29] S.A. Zaidi, A. Umar, S. Baskoutas, H. Bouzid, A.A. Ibrahim, G.N. Dar, et al., Growth and properties of Ag-doped ZnO nanoflowers for highly sensitive phenyl hydrazine chemical sensor application, Talanta 93 (2012) 257−263.

[30] K.J. Stevenson, J.L. Lyon, Z.V. Feng, R.M. Crooks, J.S. Croley, D.A. Vanden Bout, Synthesis and catalytic evaluation of dendrimer-encapsulated Cu nanoparticles. An undergraduate experiment exploring catalytic nanomaterials, J. Chem. Educ. 86 (2009) 368.

https://doi.org/10.1016/j.heliyon.2019.e01475

[31] S. Pat, M.Z. Balba, Ş. Korkmaz, Mechanical properties of deposited carbon thin films on sapphire substrates using atomic force microscopy (AFM), Ceram. Int. 40 (2014) 10159−10162.

[32] Z. Zeng, J.C. Tan, AFM nanoindentation to quantify mechanical properties of nano- and micron-sized crystals of a metal-organic framework material, ACS Appl. Mater. Interfaces 9 (2017) 39839−39854.

[33] L. Shang, K. Nienhaus, G.U. Nienhaus, Engineered nanoparticles interacting with cells: size matters, J. Nanobiotechnol. 12 (2014) 5.

[34] M.A. Sani, A. Ehsani, Nanoparticles and their antimicrobial properties against pathogens including bacteria, fungi, parasites and viruses, Microb. Pathog. (2018).

[35] Y. Qiao, F. Ma, C. Liu, B. Zhou, Q. Wei, W. Li, et al., Near-infrared laser-excited nanoparticles to eradicate multidrug-resistant bacteria and promote wound healing, ACS Appl. Mater. Interfaces 10 (2018) 193−206.

[36] A.A. Ashkarran, M. Ghavami, H. Aghaverdi, P. Stroeve, M. Mahmoudi, Bacterial effects and protein corona evaluations: crucial ignored factors in the prediction of bio-efficacy of various forms of silver nanoparticles, Chem. Res. Toxicol. 25 (2012) 1231−1242.

[37] T. Jan, J. Iqbal, M. Ismail, Q. Mansoor, A. Mahmood, A. Ahmad, Eradication of multi-drug resistant bacteria by Ni doped ZnO nanorods: structural, Raman and optical characteristics, Appl. Surf. Sci. 308 (2014) 75−81.

[38] Y. Zhu, M. Ramasamy, D.K. Yi, Antibacterial activity of ordered gold nanorod arrays, ACS Appl. Mater. Interfaces 6 (2014) 15078−15085.

[39] Y. He, P. Basnet, S.E.H. Murph, Y. Zhao, Ag nanoparticle embedded TiO2 composite nanorod arrays fabricated by oblique angle deposition: toward plasmonic photocatalysis, ACS Appl. Mater. Interfaces 5 (2013) 11818−11827.

https://doi.org/10.1016/j.heliyon.2019.e01475